Journal of Power Sources 196 (2011) 523–529

Contents lists available at ScienceDirect

Journal of Power Sources

journal homepage: www.elsevier.com/locate/jpowsour

Investigation of the impact of stacking pressure on a double-layer supercapacitor

Gerald Gourdin[a], Alexa Meehan[a], Thomas Jiang[b], Patricia Smith[b], Deyang Qu[a,*]

[a] Department of Chemistry, University of Massachusetts Boston, 100 Morrissey Blvd., Boston, MA 02135, United States
[b] Naval Surface Warfare Center, Carderock Division, 9500 MacArthur Blvd., West Bethesda, MD 20817, United States

ARTICLE INFO

Article history:
Received 9 April 2010
Received in revised form 6 June 2010
Accepted 9 June 2010
Available online 16 June 2010

Keywords:
Supercapacitor
Stacking pressure
Access surface
Transmission line model
Impedance

ABSTRACT

There are two important steps necessary for the optimization of electrochemical double-layer capacitors (EDLC): maximizing the volumetric capacitance and minimizing the ohmic resistance. The application of force during the assembly of an EDLC cell is one way to achieve this optimization. The effect of the application of force on the performance characteristics of EDLC cells, assembled using porous activated carbon electrodes, was determined. It was shown that applying force to the body of the cell during assembly only provides a significant increase in the performance of the EDLC with the initial application. The results showed that any increase in the applied force beyond that initial stage does not result in a subsequent increase in performance and can result in a substantial decrease in the performance characteristics of the EDLC cell. Furthermore, it was concluded that the substantial decrease shown was attributed to an alteration of the physical structure of the porous material, which produced significant decreases in the accessible surface area and the material resistance of the activated carbon electrodes.

1. Introduction

There is a growing need for specialized electrochemical energy storage devices for which a part of that can be met by electrochemical double-layer capacitors (EDLC) or supercapacitors. The power delivery performance of an EDLC fills the gap between dielectric capacitors and traditional batteries which makes them well suited for time-dependent electrical power output applications [1], such as memory backup [2], cold-start vehicle assist [3], and solar cell power storage [4]. Furthermore, EDLCs also have potential as high-power energy sources that can supplement the traditional energy sources for powering trains [4] and electric vehicles [4,5]. In any advanced application such as these, excellent rate performance and high capacitance are necessary requirements.

The energy storage mechanism of EDLCs derives from the formation of an electric double layer at the electrode/electrolyte interface [6], which is what provides the high-power capability of these systems. This electrostatic (non-faradaic) separation of charge also provides an EDLC with an exceptionally high rate of recyclability, nearly hundreds of thousands cycles, without any noticeable degradation of performance. This is in contrast to secondary batteries, whose recyclability is far more limited. They are required to undergo repeated chemical changes as part of their operation, which results in a significant degradation of the electrode materials over repeated charge/discharge cycles. However, as a consequence of the nature of reversible electrostatic charging, EDLC systems suffer from a more limited energy density as compared to typical batteries [2,6].

As with any specialized device, EDLC cells should first be optimized for their desired application. To obtain optimal performance from an EDLC, there are two important factors to consider: volumetric capacitance and ohmic resistance. The volumetric capacitance is the capacitance per unit bulk volume of electrode material and an important first step in achieving a high volumetric capacitance for any type of electrode material is to minimize the distance between the working and counter electrodes [1]. The other important factor, the ohmic resistance or equivalent series resistance (ESR), can be reduced through improved physical contact between the electrodes and the porous separator [4]. For a sealed cell, both of these factors can be addressed by applying force to the body of the cell during assembly to bring the electrodes into strong, direct contact with both the porous separator and the current collectors.

Certain observations can be made if capacitors are separated into two general types. Simple capacitors can be described as those that are constructed using flat plate electrodes separated by a dielectric [6]. Any potential consequences that may arise from the application of force during the construction of this type of capacitor are not significant. However, unlike simple dielectric capacitors, activated carbon is the preferred material for EDLC electrodes [7,8]. Activated carbon materials possess the high electric conductivity and large specific surface area that is essential for the development of high charge-storage capacitors [9,10]. However, activated carbon materials are highly porous and compressible [11] and so the use

* Corresponding author. Tel.: +1 617 287 6036; fax: +1 617 287 6185.
E-mail address: deyang.qu@umb.edu (D. Qu).

0378-7753/$ – see front matter © 2010 Elsevier B.V. All rights reserved.
doi:10.1016/j.jpowsour.2010.06.022

of these materials as the electrodes presents a more complicated situation than simple plate electrodes.

The most apparent negative consequence to the performance of the supercapacitor is that the pressure could change the morphology of both the porous electrodes and the separator. Activated carbon materials are highly porous and compressible [11]. It is possible with the application of sufficient force that carbon material electrodes would compress, possibly altering the physical structure of the material. This has two potential consequences for the operation of an EDLC cell, which may not be evident outside that particular environment: (1) a displacement of the electrolyte away from contact with the surface of the carbon electrodes and (2) a significant decrease in the accessible surface area of the carbon material due to the restriction of the transport channels [10]. Since it is well established that the extant of accessible surface area and the pore size distribution of activated carbons influence EDLC performance [7,12], the loss of accessible surface area and the displacement of electrolyte could result in a significant impact on the performance characteristics of the electrochemical capacitor [13,14]. This gives rise to the question as to what is the limit, if any, to how much force could be applied to a cell.

Possible evidence to this effect was exhibited during the assembly of an EDLC cell. The typical procedure for assembling an electrochemical cell is to decrease the gap between the two identical activated carbon electrodes in a stepwise fashion. The cell is typically sealed so that when the gap is decreased by a certain fixed amount, the resultant decrease in volume in the internal chamber, which houses the electrodes and separator, compresses the electrolyte producing a small pressure on both electrodes. Tests were performed on the cell before the pressure had been released and then compared to tests performed after the release of that pressure. Fig. 1 shows the cyclic voltammetry measurements of a supercapacitor cell taken before and after the release of pressure. These data indicate that the cell showed less favorable performance when the electrodes were under pressure than when the pressure within that cell had been released. This phenomenon could be attributed to the alteration of the porosity of the electrode or the separator.

The effect of increasing applied force during the assembly of an EDLC prepared using activated carbon material electrodes was investigated. The work focused specifically on the effect of the application of force on the performance characteristics of the cell. The assembled electrochemical cells were subjected to increasing force to minimize the gap between the electrodes and maximize the contact with the separator. The performance characteristics of the EDLC cells were determined at different stages during the process. Two standard electrochemical methods, cyclic voltammetry and AC impedance analysis, were used in these studies to determine the performance capabilities of the EDLC cells under different conditions.

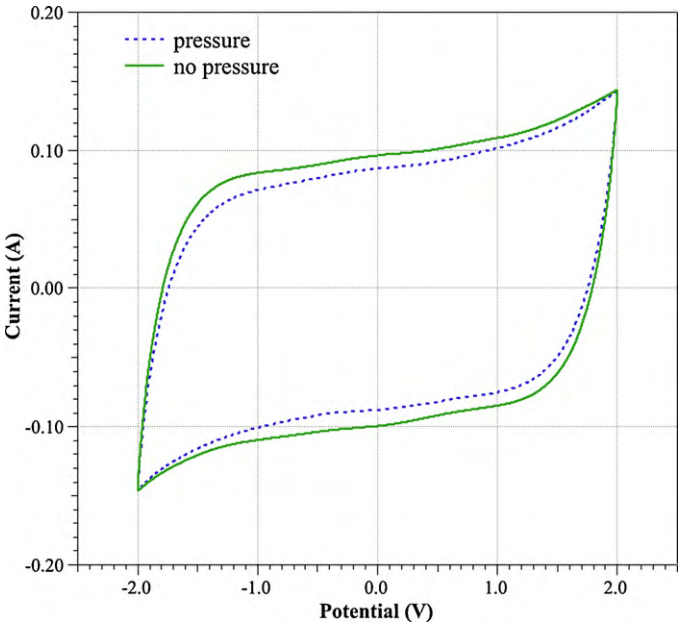

Fig. 1. Exp P3: cyclic voltammetry measurements of an EDLC cell taken before and after release of pressure.

Table 1
Typical specifications for single electrode.

Thickness	0.00125″ (0.0318 mm)
Diameter	0.6941″ (17.63 mm)
Area	2.441 cm^2
Total Mass	0.08895 g
Ni mesh	0.06444 g
Carbon (only)	0.02451 g
BET Specific surface area (YP-17D)	1516 $m^2 g^{-1}$
BET Specific surface area (M-20)	2100 $m^2 g^{-1}$ [15]

2. Experimental

2.1. Construction of the electrodes

Activated carbon materials were purchased from Kuraray Chemical (YP-17D) and SpectraCorp USA (M-20). The carbon electrodes were prepared by dispersing a Teflon (DuPont T-60) binder into the powdered activated carbon at a concentration of 1% by mass. The prepared dough was subsequently hot molded to a flexible film using a roller press set to a final thickness of 0.005″ (0.127 mm). The resulting carbon film was laminated onto a Ni mesh (4Ni 7-100AN, Dexmet Corporation) using a heavy-duty roller press set to a final thickness of 0.002″ (0.051 mm). Electrodes were punched out of the laminated material, dried at 120 °C under vacuum for 18 h, and then stored under an inert (argon) atmosphere until required. The attributes for an average electrode were determined by taking the average of 12 electrodes and are reported in Table 1.

2.2. Electrochemical cell

Electrochemical cells were constructed to perform the electrochemical measurements. The design of the cell allows the carbon electrode to be studied in two configurations: (1) a typical three-electrode configuration and (2) a face-to-face two-carbon electrode configuration representative of a commercially manufactured capacitor. A porous polymeric membrane (C200, Celgard) was used as the separator and 1 M tetraethylammonium tetrafluoroborate (TEATFB) in acetonitrile was chosen as the electrolyte [16,17]. The same type of carbon electrode was used for both the working and counter electrodes in case three-electrode measurements were performed. The design of the electrochemical cell is shown in Fig. 2.

For each experiment, the cell was assembled under an argon atmosphere. Prior to assembly, the porous separator was immersed in a small amount of electrolyte. A small quantity (200 μL) of the electrolyte, 1 M TEATFB/ACN, was added to each cell half to wet the reference electrode and the supporting nickel base current collectors. The carbon electrodes were placed in position on the nickel current collectors and each wetted with 100 μL of the electrolyte. An additional 200 μL of electrolyte was added to the larger cell half. The wetted porous separator was placed in position on one of the electrodes and the two cell halves assembled. An additional 500 μL of electrolyte was transferred into the cell cavity through the ventilation hole. The total volume of electrolyte in the cell depended

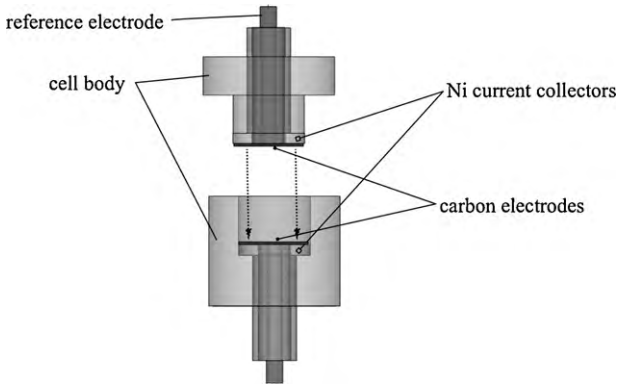

Fig. 2. Schematic view of EDLC cell. Cell body is constructed of Teflon.

on the configuration of the cell (see below). The gap between the two cell halves was reduced in steps using stainless steel shims of fixed sizes to control the degree of reduction in the gap distance between the two cell halves. After each reduction, the pressure within the cell was released by loosening the vent screw. This procedure allowed the electrodes within the cell to experience a slight pressure during assembly, while also preventing that pressure from becoming high enough to damage the electrodes or separator.

The internal configuration of the cell was altered for the force testing experiments by inserting three or four nickel spacers (0.010″) between one of the nickel current collectors and its Teflon base. This design allowed the decrease in the internal gap between the working and counter electrodes to be determined externally while an external force was applied to the cell. The external gap between the two cell halves was used to calculate the internal gap between the two electrodes using Eq. (1). The EDLC cell was then assembled using the stepwise procedure, while accounting for the increased spacing between the two electrodes introduced with the addition of the spacers. The addition of the nickel spacers increased the volume capacity of the cell and so an additional 200 μL of electrolyte was added to the cell. A cell was considered completely closed when the gap between the two cell halves was 0.000″ or equal to the combined thickness of the spacers that were added prior to assembly (0.030″ or 0.040″). This stage marked the starting point for all experiments. The internal gap values reported in this paper represent calculated distances between the surfaces of the two carbon electrodes.

$$Gap_{\mathrm{mm}} = \left(Gap_{in} - SP_h \cdot f + 0.37'' - h_E \cdot 2\right) 25.4 \frac{\mathrm{mm}}{\mathrm{in}} \quad (1)$$

where Gap_{in} is the external gap between two cell halves (inches); SP_h is the height of spacers added to interior of the cell (inches); f is the factor to account for air gaps between stacked spacers, and $f = 1.38$ (3 spacers), $f = 1.48$ (4 spacers); h_E is the average thickness of carbon electrode; 0.37″ is the natural gap between Ni current collectors.

2.3. Experimental techniques and instrumental details

Linear sweep cyclic voltammetry tests were carried out on a cell in the two-electrode configuration using an Ecochemie potentiostat/galvanostat (Autolab PGSTA 30) under a scan rate of 100 mV s^{-1} and through a potential range of −2.0 to +2.0 V. Electrochemical impedance spectroscopy measurements were also carried out using the same instrument with the frequency analyzer (FRA2) module set to a frequency range of 100 mHz to 10 kHz. The instrument was computer controlled for both tests using the Nova software (version 1.5), as provided by Ecochemie. All equivalent circuit fittings of the AC impedance data were performed using the built-in tools of the Nova software.

2.4. Applied force conditions

To determine the conditions the cell has to be under to induce a 'collapse' of an electrode, force was applied to an assembled cell using a vertical hand wheel Force Testing stand (IMADA model HV-110S) equipped with a digital force gauge (IMADA model DS2). The cells used in these experiments were altered through the addition of the nickel spacers, as described above. A cell was assembled to its initial starting state and then force was applied to reduce the gap between the two cell halves of the cell. This had the effect of decreasing the volumetric capacity of the cell cavity and increasing the pressure on the working and counter electrodes. In these experiments the pressure within the cell was not released. The decrease in the gap distance between the two cell halves was controlled through the use of stainless steel shims of fixed size. Linear scan cyclic voltammetry and FRA impedance measurements were performed at each stage in the process. The force applied to the cell and the gap between the two cell halves was also measured.

Due to the limitations of the Force Testing stand and the design of the cells, another set of experiments was performed without the use of the Force Testing stand. Instead a hand clamp was used to apply force to an assembled cell. As before, stainless steel shims were used to control the gap distance between the two cell halves. Linear scan cyclic voltammetry and FRA impedance measurements were performed at each stage in the process and the gap between the two cell halves was recorded. If the measurements indicated that the one or both of the carbon electrodes had 'collapsed', then the pressure on the cell was immediately released.

3. Results and discussions

A total of 12 experiments were performed. Three of the experiments directly compared the differences in the performance characteristics of a cell while under pressure and while not under pressure. At each stage during the assembly of a cell, two measurements were taken: (1) after a decrease in the gap between the two cell halves, which produces an increase in pressure within the cell compartment and (2) after that pressure within the compartment was released. All experiments exhibited behaviors as represented in Fig. 1. The remaining nine experiments examined the effect of increasing pressure on the performance characteristics of the EDLC cell. Five of those experiments used the Force Testing apparatus to apply a measured amount of force and the remaining four experiments used a hand clamp to apply pressure to the cell. A list of all the experiments performed is presented in Table 2.

3.1. Cyclic voltammetry measurements

A cyclic voltammetry (CV) measurement of an ideal EDLC operating in the two-electrode configuration should produce a

Table 2
Experiment list.

Experiment ID	Type	Carbon ID
P1	Pressure/no pressure comparison	YP-17D
P2		YP-17D
P3		YP-17D
F1	Force stand	YP-17D
F2		YP-17D
F3		YP-17D
F4		YP-17D
F5		YP-17D
C1	Hand clamp	YP-17D
C2		M-20
C3		YP-17D
C4		YP-17D

symmetric voltammogram, which means that the portion of the plot associated with discharging of the EDLC is a mirror image of the portion of the plot generated during charging of the cell. This produces a voltammogram that is generally rectangular in shape [6]. This type of behavior is illustrated in Fig. 1, which shows that the current is constant for a constant sweep rate of potential since it is directly related to the capacitance, as shown in Eq. (2) [5,18,19].

$$q = C \cdot V \Rightarrow \frac{\delta}{\delta t} q = \frac{\delta}{\delta t} (C \cdot V)$$
$$\frac{\delta q}{\delta t} = I = C \frac{\delta}{\delta t} V \tag{2}$$
$$I = C \cdot s$$

where I is the current, C represents the total capacitance and s stands for the potential sweep rate in Vs^{-1}.

By comparing the CVs of the same cell under different pressured states, certain assumptions regarding the total capacitances associated with the cell can be made. The degree of rectangularity in a CV is an indication of how close the performance of a supercapacitor approaches that of an ideal capacitor: the less rectangular the CV, the more the supercapacitor cell is dominated by resistive behavior. Additionally it can be inferred that the magnitude of the sum of the absolute values of the charging current and the discharging current is representative of the total capacitance for the cell. An increase in that difference corresponds to an increase in the total capacitance for the cell, when the CVs are performed under the same constant scan rate. Although a calculated 'Magnitude' value should not be equated with the actual capacitance of a cell, this value can be used to quantitatively compare the different CVs of a particular cell obtained under different conditions. In this work, a 'Magnitude' value was calculated using Eq. (3).

$$M_0 = \left|I_0^+\right| + \left|I_0^-\right| \tag{3}$$

where $I_o{}^+$ is the current at $V = 0$ during charging of the capacitor, $I_o{}^-$ is the current at $V = 0$ during discharging of the capacitor and M_o is the magnitude.

Two significant behaviors were observed in the CV measurements of the EDLC cells used in these experiments. The results of the force experiments showed that as more force was applied to an EDLC cell, the magnitude (M_0) increased until a maximum value was reached. After which the current difference, or magnitude, would either stop increasing and maintain a relatively constant value, or decrease as the force applied to the cell increased.

The typical cyclic voltammograms that were acquired in all experiments were similar to those illustrated in Fig. 1. The CV measurements that constitute a set for each experiment were obtained after the gap between the cell halves was reduced by a fixed amount, as described above. This reduction corresponds to a decrease in the internal gap between the two electrodes and an increase in the internal pressure. The internal gap and magnitude values were calculated using Eqs. (1) and (3), respectively, for each CV measurement from experiment C1 and are listed below in Table 3.

The data in Table 3 demonstrate that, with decreases in the internal gap of the cell, the M_0 (magnitude) value will at first increase, and then steadily decrease as the internal gap distance decreases. This implies that the application of force to the cell will produce an increase in the performance characteristics of a cell, as qualified by M_0, but only for the application of a limited amount of force. These same calculations were performed for experiments F1, F3, F4, C2, C3, and C4 and those results are presented in Fig. 3. Despite the differences in the calculated M_0 values, those experiments exhibited the same overall behavior. The plots show only an initial increase in the M_0 value followed by a decrease in that value as the internal gap distance decreases.

Table 3
M_0 Values for different tests from Exp C1.

Gap_{in}	Gap_{mm}	M_0
0.030	0.015	0.29816
0.027	−0.061	0.29834
0.025	−0.112	0.29746
0.022	−0.188	0.29746
0.020	−0.239	0.29440
0.018	−0.290	0.29450
0.015	−0.366	0.29398
0.012	−0.442	0.29370
0.010	−0.493	0.29355
0.008	−0.544	0.29303
0.005	−0.620	0.29337
0.002	−0.696	0.29392

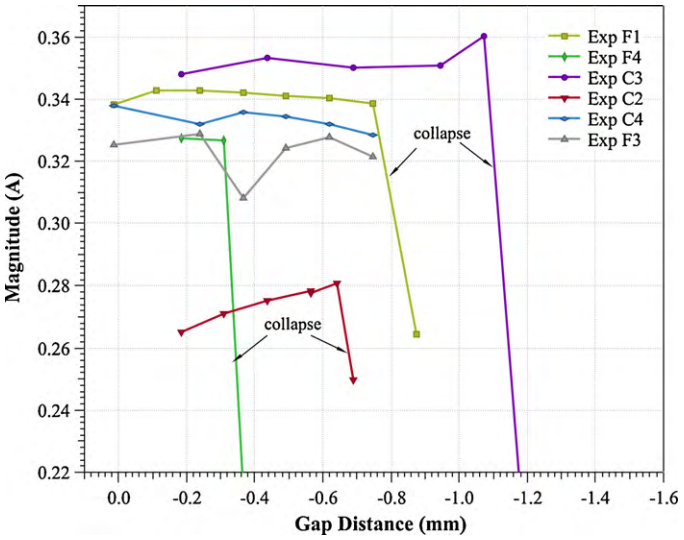

Fig. 3. Magnitude, M_0, vs. internal gap distance plots for a selection of experiments. Experiments that exhibited significant drops in performance due to a 'collapse' of the electrode are identified.

The other significant behavior observed can be described as a 'collapse' of the CV scan. This is noted by a dramatic alteration of the CV scan away from the rectangular shape that is normally associated with capacitive behavior and more towards a skewed linear shape that is indicative of resistive behavior that more closely follows Ohm's law: $V = IR$. The state at which the CV departs from the expected behavior represents a 'collapse' of one, or both, of the carbon electrodes or the separator. This alteration of the CV was exhibited in four of the nine experiments where force was applied to the cell (see Table 4). The altered CV measurements from two of these experiments, C2 and F1, are shown in Fig. 4. The CVs obtained from the other two experiments, although not shown, were very similar. The results in Fig. 4 show that CVs produced by EDLC cells in this 'collapsed' state demonstrate a significant drop in capacitance of the cell, producing an almost direct correlation between potential and current. This indicates that cells in that state are dominated more by resistive behavior than by capacitive

Table 4
M_0 values for experiments in the 'collapse' state.

Exp ID	Applied force[a] (N)	Gap_{mm}	Final M_0
F1	1984	−0.747	0.2644
F4	467	−0.437	0.0497
C2	>920	−0.640	0.2499
C3	2175	−1.079	0.1884

[a] Applied force' and Gap_{mm} are the amount of force applied and the calculated internal gap, respectively, at the step before the cell entered a 'collapsed' state.

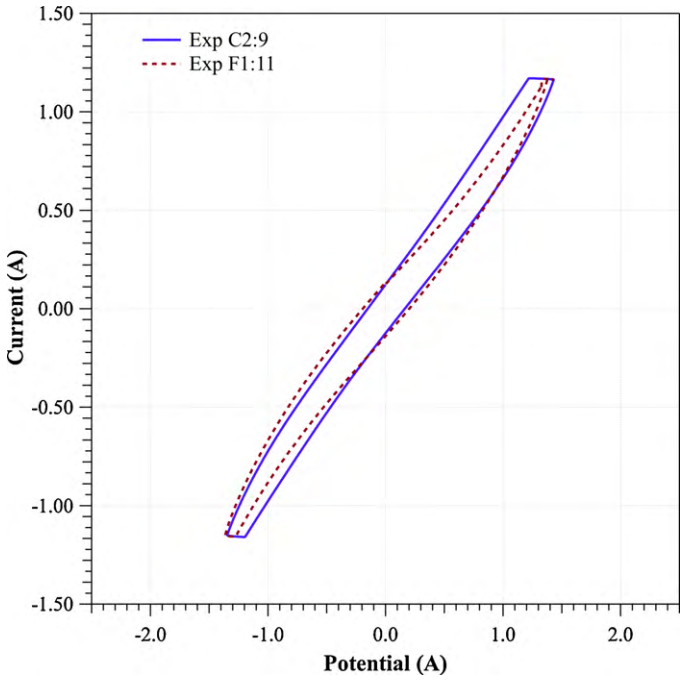

Fig. 4. Cyclic voltammetry measurements of Exp C2, Test 9 and Exp F1, Test 11.

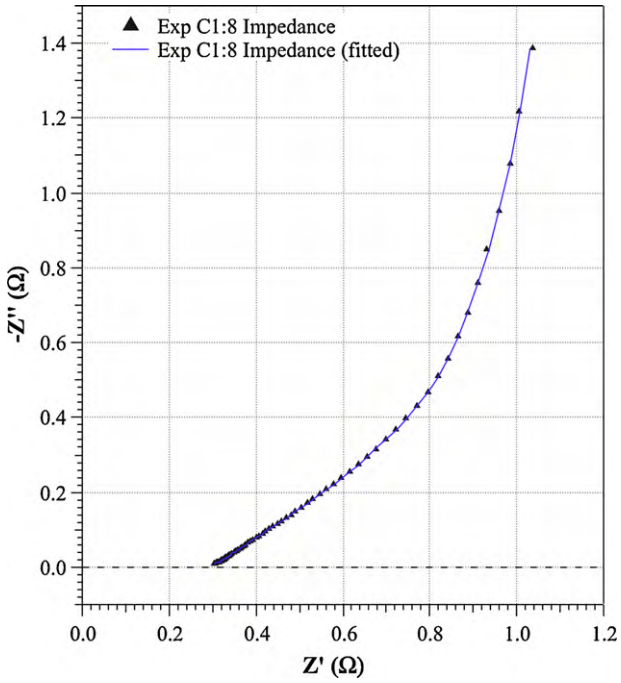

Fig. 6. AC impedance responses for activated carbon electrode in Test 8 of experiment C1. Numerical fitting was based on the equivalent circuit shown in Fig. 4. Most experiments gave similar results except those already noted in the test.

behavior. The failure of the supercapacitor at high pressure could come as a result of a failing of the separator, i.e. penetration of the separator or electrolyte starving within the separator, which was caused by the increase in internal pressure. However, the graphs still show a gap between the charging and discharging curves, indicating that the EDLC cell still exhibits some capacitance. This implies that the separator has not completely failed and is still partially functional. Table 4 lists the final M_0 value and other relevant data points associated with the previously described experiments at the stage the cell entered a 'collapsed' state.

3.2. Comparison of distributed capacitances by AC impedance

The impedance response of an EDLC constructed with porous electrodes can be modeled using an equivalent circuit representation of a truncated transmission line [6,20]. The transmission line model is a distributed network that consists of n resistor–capacitor (RC) loops, as represented in Fig. 5. Since the mathematical equation of the transmission line model has the same form as the diffusion equation, the process taking place within an RC circuit may be treated as electronic diffusion into a semi-infinite medium [15]. Therefore, the modeled response of an RC transmission line network can be analogous to the depth an AC signal may penetrate with respect to the depth of the pores in a porous electrode.

In this study, the transmission line with infinite RC loops was simplified to an 8-loop transmission line model. In that simplified model, one can consider each RC loop as representing 1/8 of the total accessible surface area of a porous carbon electrode. The impedance data generated for these experiments were fitted using an 8-loop model. The impedance data for one measurement from experiment C1 is presented in Fig. 6 in the form of a complex impedance plot. The fitting obtained using the 8-loop transmission model is also shown in Fig. 6 and it is obvious that the model fits the impedance data very well. These data are typical for each measurement in all experiments, except where the cell had entered a 'collapsed' state. Since the capacitor elements are arranged in parallel in the transmission line model (Fig. 5), the total capacitance for the cell can be calculated by summing up the capacitance values for each of the sub-capacitors in the network. The total capacitance and specific capacitance were calculated using Eqs. (4) and (5), where wt is the weight of the carbon for one electrode obtained from Table 1.

$$C_{tot} = C_1 + C_2 + C_3 + C_4 + C_5 + C_6 + C_7 + C_8 \quad (4)$$

$$C_{spec} = \frac{C_{tot}}{wt} = \frac{C_{tot}}{0.02451\ \text{g}} \quad (5)$$

Fig. 7 shows a plot of the specific capacitance values as a function of the internal gap distance for experiments C1, C2, C3, F2, and F5. Each experiment plotted in that figure shows an initial, but limited, increase in the specific capacitance of a cell as the internal gap distance decreases. These results are a reflection of the behavior seen with the M_0 data and are further evidence that the addition of some pressure to a cell does result in an improvement of its performance characteristics, but only to a limited extent. Additional pressure to a cell does not seem to offer any improvement and, in most cases, can negatively affect its performance capabilities, as measured by the specific capacitance, even to the extent of a sudden failure of the supercapacitor. The "▼" markers in Fig. 7 indicate the point of maximum specific capacitance for each experiment with the over-

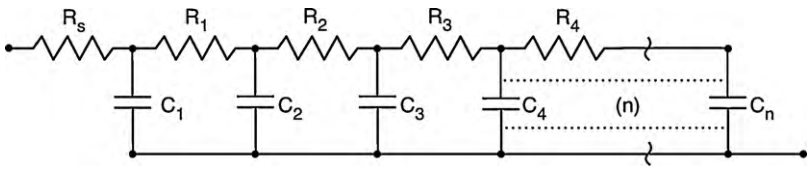

Fig. 5. Truncated transmission line network used for modeling the impedance behavior of porous material electrodes.

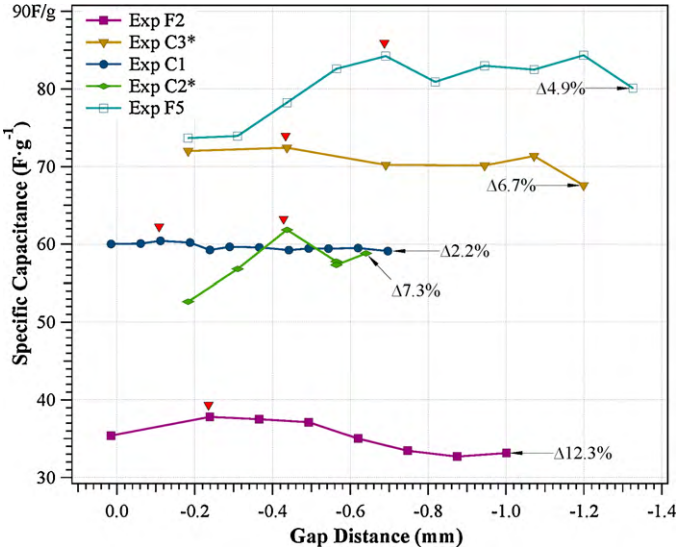

Fig. 7. Specific capacitance vs. internal gap distance plots for a selection of experiments. Maximum specific capacitance (red marker) and overall decrease in capacitance from the maximum are indicated. (For interpretation of the references to color in this figure legend, the reader is referred to the web version of this article.)

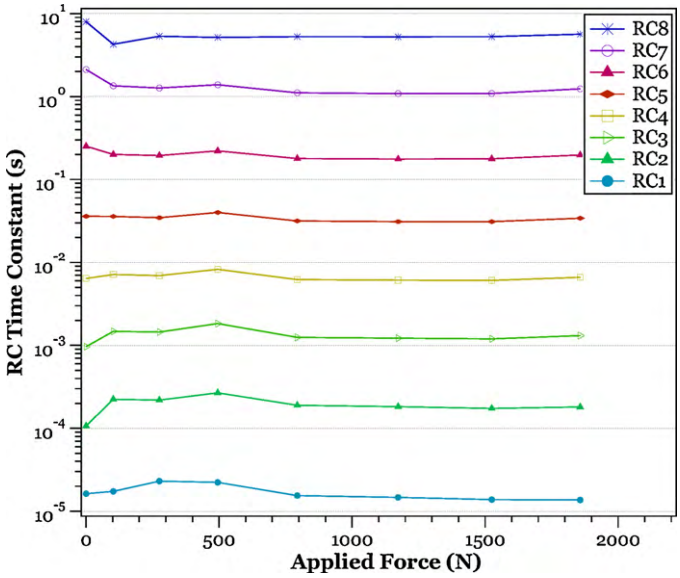

Fig. 9. RC time constants as a function of the applied force obtained from experiment F2.

all percentage decrease in specific capacitance noted at the end of each plot.

It has previously been established that the different pore sizes in a porous electrode will have different time constants [8]. This implies that not all of the accessible surface area of a porous electrode can be accessed within the same time frame. Thus, the total capacitance will depend on the density of the charge or discharge current. In addition, certain behaviors will arise as a result of the finite resistance of the particles, the supporting electrolyte, and the inter-particle contact resistance. The root causes of these phenomena are attributed to the inhomogeneity of the porous electrode material. Therefore, the ionic diffusion rates inside the different sized pores will vary, and so the double layers established on the surface of the pores will also have different response times to the modulating frequency of the AC signal. The surface area of the smaller pores will be projected by the lower frequency modulating signals. Therefore, an AC impedance analysis using the transmission line model is a good approach to evaluating the time-dependence characteristics of a porous electrode. In the simplified 8-loop transmission line model, the indices of the different sub-capacitors correlate inversely to the accessible surface area associated with the different sized pores, largest to smallest. The change in the capacitance of each individual sub-capacitor will represent a change in the projected surface area under different conditions. Figs. 8 and 9 show two graphs derived from the impedance data obtained from experiment F2. Fig. 8 shows two plots of the capacitance values of the individual sub-capacitors as a percentage of the total capacitance. The figure is split into two plots to more clearly present the results from each measurement in the experiment. Fig. 9 shows a semi-log plot of the RC time constants as calculated. RC time constants represent the time for modulation signals to reach the internal surface areas from the orifices of the pores. Both figures are plotted as a function of the applied force.

It is important to note the changes in the distribution of the total capacitance among the various pores sizes as illustrated in Fig. 8. It can be seen that when there is no applied force, the surface areas of the mesopores and micropores contributed to the majority of the distributed capacitance, since the sub-capacitors associated with those pores, Caps 5–8, represent more than 90% of the total capacitance. After an increase in the stacking pressure, the distribution of capacitance among those four distributed sub-capacitors changed, although the total contribution of Caps 5–8 still accounted for more than 90% of the total capacitance. Fig. 8 shows that the share of the total capacitance from Caps 5–7 decreased as the stacking pressure increased, while the share from Cap 8 increased. This share repre-

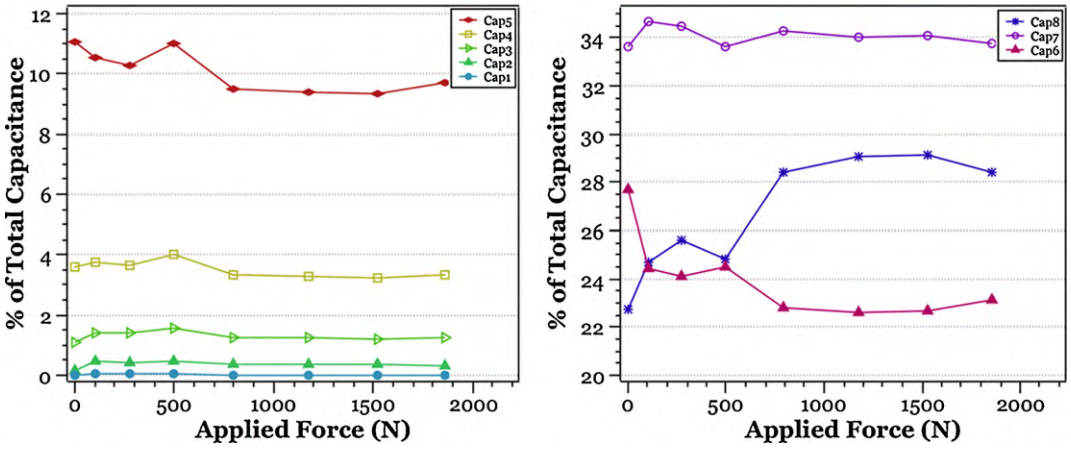

Fig. 8. Capacitance values (% of total) of the individual sub-capacitors as a function of the applied force obtained from experiment F2.

sents the 1/8 fraction of the total accessible surface area contributed by the smallest pores. This change in the distributed capacitance distribution could be caused by an alteration in the accessible surface area of the various sized pores. It would appear, then, that the electrochemical accessibility to the mesopores and the larger sized micropores has decreased, which could come as a result of the loss of electrolyte from within those pores. However, the accessibility to the smaller sized micropores did not change as evidenced by the increase in the share of the total capacitance associated with Cap 8. These results could be attributed to the "pore-filling" effect, which would imply that the electrolyte within the micropores would not be squeezed out by the increase in the stacking pressure.

As shown in Fig. 9, the RC time constant for each RC loop also decreased with an increase in the stacking pressure. This implies that there was an improvement in the kinetics of the electrochemical accessibility to the surface area of the smaller pores. Therefore, it appears that increasing the stacking pressure reduces the distributed resistance within the electrode porous matrix by improving particle-to-particle contact.

The cyclic voltammograms in certain experiments indicated that one, or both, of the carbon electrodes had entered what was described earlier as a 'collapsed' state. The impedance data associated with those experiments differed significantly from what is considered the normal impedance behavior of an EDLC, as shown in Fig. 6 [4,6,21]. A brief evaluation of the post-collapse data indicates that the distributed capacitance values are significant only at very low modulating frequencies and decrease quite rapidly to values well below those obtained from the cells in the pre-collapse state as the frequency increases. In addition, the total resistance values are only a fraction of the resistance values exhibited in the pre-collapse cells. This analysis can clearly account for the electrochemical behavior of the post-collapse cells, as illustrated by the CVs in Fig. 4. In effect, after the application of sufficient force, the cells exhibited a significant reduction in total capacitance and a substantially diminished resistance that gave rise to cell currents that correlate strongly with the applied potential.

A substantial decrease in capacitance, as observed in these experiments, could come as the result of a decrease in the total accessible surface area of the electrode. The total surface area of an electrode is solely dependent on the degree of porosity of the material. Under sufficient pressure, it would be expected that the physical dimensions of the transport channels within the electrode material would shrink, or perhaps be sealed, and that the overall accessibility of the pore cavities would decrease. This process would not only decrease the overall capacitance, due to the decrease in the accessible surface area, but also the resistance associated with pore depth. As the accessible surface area sharply decreases, the distributed capacitance drops and, based on the transmission line model, the device then responds to the sweep potential with resistor-like behavior. Similar arguments could also be made for the separator, for as the electrolyte is squeezed out, a now 'dry' separator could not provide sufficient ionic conductivity and the device would thus behave more like a resistor. Further analysis to pinpoint the cause of such a drastic 'collapse' is currently in progress and those results will be reported later.

Not addressed here, but of equal importance, is the degree of which an electrode may or may not recover out of its 'collapsed' state. Experiments unrelated to the work presented here indicate that a carbon electrode can recover out of its 'collapsed' state and return to a state of near-optimal performance, after the release of the stacking pressure. That "recovery" phenomenon is significant because it would rule out the possibility of penetration of the separator, or at least in the cases of those cells that could recover to close to their original performance. Any variation in the degree of recoverability of electrodes manufactured from different types of activated carbon also needs to be explored in additional research.

4. Conclusion

The goal of this work was to determine what effect the application of force during the assembly of an EDLC would have on the performance characteristics of a cell. Since force is routinely used to assemble electrochemical cells to minimize the gap between the electrodes and maximize the contact with the separator, the question as to what are the limits to how much force could be applied to an EDLC cell is an important one.

The results presented in this work indicate that the application of increasing force on an EDLC cell only provides a limited increase in the capacitance of the device, after which any additional force does not provide any significant improvement. Furthermore, under certain high-pressured conditions, the behavior of the EDLC cell demonstrated a substantial drop in performance of the cell and that it can be concluded that the application of force altered the physical structure of the activated carbon electrodes resulting in a decrease in the accessible surface area and a displacement of the electrolyte [13]. The AC impedance response of an electrode in this state supports these conclusions as seen by the change in the distribution of the total capacitance and the decrease in the values of the individual RC time constants. The impedance response also indicates the influence of dispersive effects at low frequencies, which is a characteristic associated with a thin, porous layer of material bonded to a thicker substrate [22]. In addition, an evaluation of the impedance data from the different experiments suggests that there may be stages to the 'collapsing' process and that this needs to be explored further.

Acknowledgement

The authors gratefully acknowledge the support from the Office of Naval Research.

References

[1] A. Burke, J. Power Sources 91 (2000) 37–50.
[2] J. Zheng, J. Huang, T. Jow, J. Electrochem. Soc. 144 (1997) 2026–2031.
[3] B.E. Conway, V. Birss, J. Wojtowicz, J. Power Sources 66 (1997) 1–14.
[4] R. Kötz, M. Carlen, Electrochim. Acta 45 (2000) 2483–2498.
[5] B.E. Conway, J. Electrochem. Soc. 138 (1991) 1539–1548.
[6] B. Conway, Electrochemical Supercapacitors: Scientific Fundamentals and Technological Applications, Springer, 1999.
[7] J. Gamby, P. Taberna, P. Simon, J. Fauvarque, J. Power Sources 101 (2001) 109–116.
[8] D. Qu, H. Shi, J. Power Sources 74 (1998) 99–107.
[9] E. Frackowiak, F. Béguin, Carbon (2001).
[10] H. Shi, Electrochim. Acta 41 (1996) 1633–1639.
[11] A. Pandolfo, A. Hollenkamp, J. Power Sources 157 (2006) 11–27.
[12] T.-C. Weng, H. Teng, J. Electrochem. Soc. 148 (2001) A368–A373.
[13] S. Alvarez, M. Blancolopez, A. Mirandaordieres, A. Fuertes, T. Centeno, Carbon 43 (2005) 866–870.
[14] Y. Maletin, P. Novak, E. Shembel, V. Izotov, N. Strizhakova, A. Mironova, V. Danilin, S. Podmogilny, Appl. Phys. A 82 (2006) 653–657.
[15] D. Qu, J. Power Sources 109 (2002) 403–411.
[16] M. Arulepp, L. Permann, J. Leis, A. Perkson, J. Power Sources 133 (2004) 320–328.
[17] K. Xu, M. Ding, T. Jow, J. Electrochem. Soc. 148 (2001) A267–A274.
[18] W. Pell, B. Conway, J. Power Sources 136 (2004) 334–345.
[19] P. Taberna, P. Simon, J. Fauvarque, J. Electrochem. Soc. 150 (2003) A292–A300.
[20] O. Barcia, E. D'Elia, I. Frateur, O. Mattos, N. Pebere, Electrochim. Acta 47 (2002) 2109–2116.
[21] P.L. Taberna, C. Portet, P. Simon, Appl. Phys. A 82 (2006) 639–646.
[22] J. Bisquert, J. Phys. Chem. B 106 (2002) 325–333.